2020

Detection of decoupled surface and bulk states in epitaxial orthorhombic SrIrO3 thin films

P. E. Evans, T. Komesu, L. Zhang, D.-F. Shao, A. J. Yost, S. Kumar, E. F. Schwier, K. Shimada, E. Y. Tsymbal, X. Hong, and P. A. Dowben

Detection of decoupled surface and bulk states in epitaxial orthorhombic $SrIrO_3$ thin films

Cite as: AIP Advances 10, 045027 (2020); doi: 10.1063/1.5135941
Submitted: 27 February 2020 • Accepted: 26 March 2020 •
Published Online: 15 April 2020

Prescott E. Evans,[1] Takashi Komesu,[1] Le Zhang,[1] Ding-Fu Shao,[1] Andrew J. Yost,[1] Shiv Kumar,[2] Eike F. Schwier,[2] Kenya Shimada,[2] Evgeny Y. Tsymbal,[1] Xia Hong,[1] and P. A. Dowben[1,a)]

AFFILIATIONS

[1]Department of Physics and Astronomy & Nebraska Center for Materials and Nanoscience, Theodore Jorgensen Hall, 855 N 16th, University of Nebraska, Lincoln, Nebraska 68588-0299, USA

[2]Hiroshima Synchrotron Radiation Center, Hiroshima University, Higashi-Hiroshima 739-0046, Japan

[a)]**Author to whom correspondence should be addressed:** pdowben1@unl.edu

ABSTRACT

We report the experimental evidence of evolving lattice distortion in high quality epitaxial orthorhombic $SrIrO_3$(001) thin films fully strained on (001) $SrTiO_3$ substrates. Angle-resolved X-ray photoemission spectroscopy studies show that the surface layer of 5 nm $SrIrO_3$ films is Sr–O terminated, and subsequent layers recover the semimetallic state, with the band structure consistent with an orthorhombic $SrIrO_3$(001) having the lattice constant of the substrate. While there is no band folding in the experimental band structure, additional super-periodicity is evident in low energy electron diffraction measurements, suggesting the emergence of a transition layer with crystal symmetry evolving from the $SrTiO_3$ substrate to the $SrIrO_3$(001) surface. Our study sheds light on the misfit relaxation mechanism in epitaxial $SrIrO_3$ thin films in the orthorhombic phase, which is metastable in bulk.

I. INTRODUCTION

The combination of strong spin–orbit interactions and electron correlation has driven the recent research interest in 5d irridates,[1–6] including the correlated semimetal $SrIrO_3$.[7–12] Orthorhombic $SrIrO_3$, as schematically shown in Figs. 1(a) and 1(b), has been theoretically predicted to host non-trivial topological phases.[10] While the crystal structure of bulk $SrIrO_3$ favors the monoclinic distortion of the hexagonal $BaTiO_3$ structure[6,13] rather than the perovskite phase, high-quality orthorhombic $SrIrO_3$(001) films have been grown on $SrTiO_3$(001),[7,9,14] $(LaAlO_3)_{0.3}(SrAl_{1/2}Ta_{1/2}O_3)_{0.7}$,[8,14] and $GdScO_3$[12] substrates. Epitaxial $SrIrO_3$ films in the ultrathin limit exhibit a range of interesting properties, including dimensionality crossover, metal–insulator transition, and enhanced spin relaxation time,[9,11,15] and it is essential to understand how the electronic structure and lattice distortion evolve in these thin films.

The goal of this research is to further examine the crystal symmetry in epitaxial orthorhombic $SrIrO_3$ thin films. This is key to any effort to exploit the interfacial charge and control quantum confinement to engineer the electronic and magnetic states in $SrIrO_3$. Furthermore, characterizing the thin film is also important to gain a deeper understanding of the finite size effects[9,11,15] for $SrIrO_3$ in this metastable phase.[10] Previous studies have shown that epitaxial $SrIrO_3$ films strained on $SrTiO_3$(001) are insulating when the films are thinner than 4 unit cells thick.[9,11,15] Obviously, thinner $SrIrO_3$(001) films are much more dominated by the surface. A key question is how the effect of the epitaxial strain is entangled with the quantum confinement in determining the electronic properties of these ultrathin films.

II. EXPERIMENTAL AND THEORETICAL METHODS

The $SrIrO_3$ thin films were grown on Ti–O terminated (001) $SrTiO_3$ and Nb doped $SrTiO_3$ (Nb:$SrTiO_3$; 0.05 wt. %) substrates using off-axis radio frequency magnetron sputtering. The films were deposited at 600 °C in 150 mTorr process gas, composed of Ar and O_2 (ratio 2:1). The detailed growth conditions can be found elsewhere.[15] We performed the surface morphology and structure characterizations on $SrIrO_3$(001) samples grown on $SrTiO_3$ substrates. The spectroscopic measurements were performed on $SrIrO_3$(001)

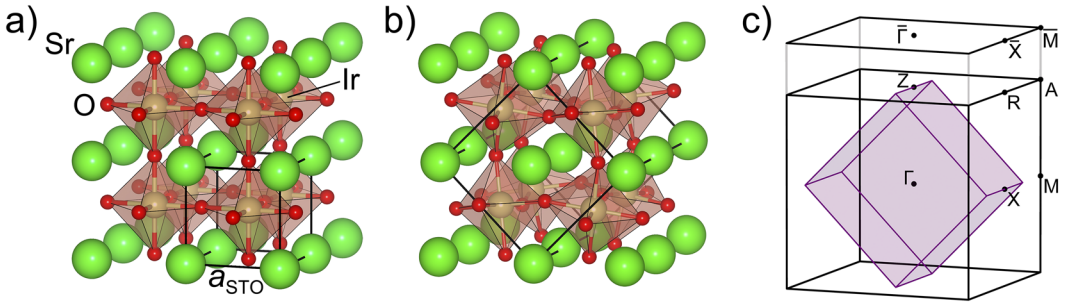

FIG. 1. (a) The schematic of the crystal structure without distortion for $SrIrO_3$ epitaxially grown on the $SrTiO_3$ substrate. The black box denotes the ideal cubic perovskite unit cell. (b) The real crystal structure of $SrIrO_3$ with octahedral distortion. The black box denotes the orthorhombic unit cell, which is enlarged by $\sqrt{2}a_0 \times 2a_0 \times \sqrt{2}a_0$ with respect to the unit cell shown in (a). (c) The Brillouin zone of orthorhombic $SrIrO_3$ (denoted by purple color), which can be unfolded into the large black Brillouin zone corresponding to the structure shown in (a). The surface Brillouin zone is shown in the top.

grown on Nb:$SrTiO_3$. After retrieving the samples from the growth chamber, the films were promptly sealed in vacuum to minimize the exposure to the ambient condition prior to the spectroscopy investigations. Four separate 5 nm samples were studied, and the results were consistent from sample to sample.

The surface morphology was examined using a Brunker Multimode 8 atomic force microscope (AFM) under the tapping mode. Figure 2(a) shows an AFM topography image of a 5 nm $SrIrO_3$(001) film, which exhibits atomically smooth terraces separated by 4 Å steps. The typical root mean square (rms) roughness is 2 Å. The structure characterizations were performed using a Rigaku SmartLab x-ray diffractometer (XRD), with a copper source ($\lambda_{K,\alpha}$ = 1.5406 Å). Figure 2(c) shows the out-of-plane XRD measurement on the same sample as in Fig. 2(a). The as-grown $SrIrO_3$ film is single crystalline with no impurity phases, and the deduced *c*-axis lattice constant is ~4.02 Å, which is consistent with the compressive strain imposed by the $SrTiO_3$(001) substrate (−1.14%). The typical rocking curves for the 5 nm films have a full-width-half-maximum of less

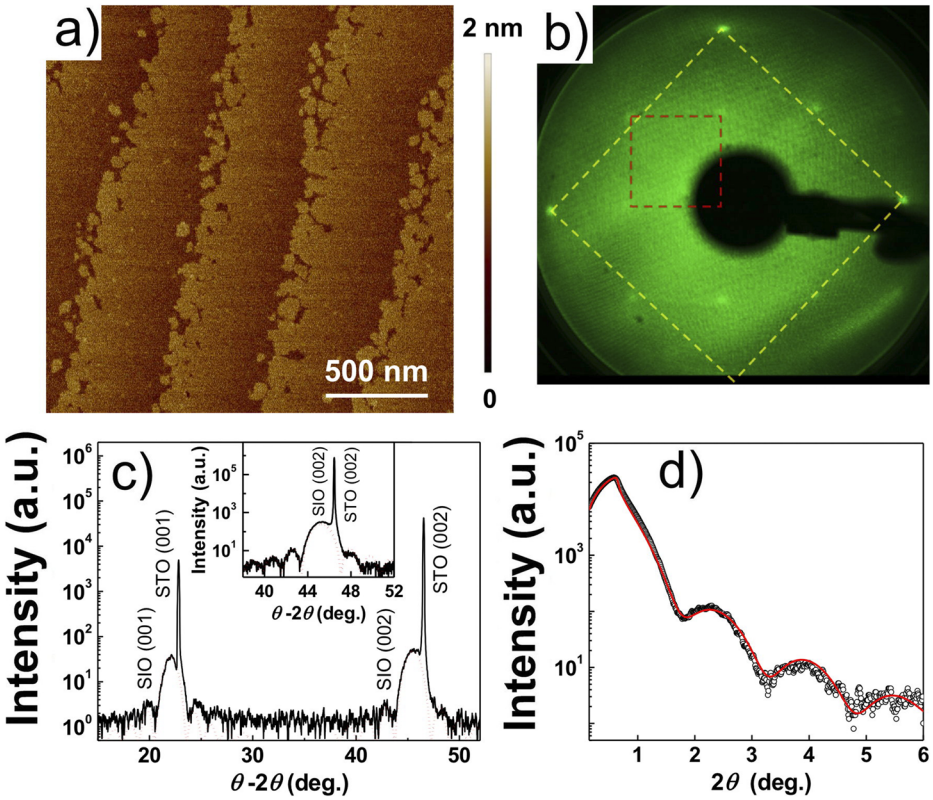

FIG. 2. (a) The atomic force microscopy (AFM) image of a 5 nm orthorhombic $SrIrO_3$(001) film grown on a $SrTiO_3$ substrate showing atomically flat terraces. The rms roughness of the film is ~2 Å. (b) The corresponding low energy electron diffraction of a 5 nm orthorhombic $SrIrO_3$(001) thin film grown on a Nb doped $SrTiO_3$ substrate. The electron energy is 31.5 eV. The yellow box highlights the reciprocal lattice of the integer order diffraction spots, while the red box highlights the faint diffraction spots due to the super-periodicity. (c) X-ray diffraction $2\theta-\theta$ scan with fits to the Laue oscillations around the Bragg peaks of $SrIrO_3$. Inset: close-up scan around the (002) peak taken on another 5 nm film. Here, $SrIrO_3$ is denoted as SIO, and $SrTiO_3$ is denoted as STO. (d) The small angle x-ray diffraction (data in black) about the $SrIrO_3$ (001) diffraction beam, with the fit to the data (red).

than 0.1°, attesting to the high crystalline quality of the samples. The film thickness was extracted by fitting to the finite-size oscillations around main Bragg peaks [Fig. 2(c), inset] and the x-ray reflectivity (XRR) measurement [Fig. 2(d)]. In a previous study,[15] using the reciprocal space mapping and pole figure techniques, we have shown that the $SrIrO_3$ films are fully strained (up to 21 nm) and conform to the four-fold symmetry of $SrTiO_3$, indicating that the films are in the orthorhombic phase.

The experimental electronic structure measurements were performed on 5 nm thick $SrIrO_3$ films using several spectroscopic methods. The high-resolution angle-resolved photoemission spectroscopy (HR-ARPES) measurements were performed on the linear undulator beamline (BL-1) of the Hiroshima Synchrotron Radiation Center (HiSOR), Hiroshima University.[16,17] We have conducted HR-ARPES using a photon energy of 150 eV in the p-polarization geometry, where the electric field vector lies in the plane of incidence as well as the photoelectron detection plane. Based on the matrix elements of the dipole transition, one can mainly detect the initial-state orbitals having even symmetry with respect to the mirror plane, which coincides with the plane of incidence. The surface stoichiometry of $SrIrO_3$(001) was established by angle-resolved x-ray photoemission spectroscopy (ARXPS), obtained using non-monochromatized Al Kα x-ray source, with a photon energy of 1486.6 eV, and a SPECS PHOIBOS 150 energy analyzer. The emission angles for ARXPS are all with respect to the surface normal. Several successive annealing steps at ~150 °C change the surface stoichiometry only slightly. Low energy electron diffraction (LEED) patterns confirming surface lattice were taken *in situ* using an Omicron SPECTALEED rear-view LEED optics system with an electron beam energy of 31.5 eV, and was seen to be very sensitive to surface preparation. The experimental band structure was compared with first-principles density functional theory (DFT) calculations, which were performed using a plane-wave pseudopotential method with fully relativistic ultrasoft pseudopotentials,[18] as implemented in Quantum-ESPRESSO.[19] The exchange and correlation effects were treated within the generalized gradient approximation (GGA).[20] In the calculation, we used the plane-wave cut-off energy of 60 Ry, and a 16 × 16 × 16 k-point mesh in the irreducible Brillouin zone. We used a $\sqrt{2}a_0 \times 2a_0 \times \sqrt{2}a_0$ orthorhombic unit cell in the calculation, with $a_0 = a_{STO}$ =3.905 Å. All the atomic coordinates were relaxed until the force on each atom was less than 0.001 eV/Å. Spin–orbit coupling was included in all electronic structure calculations. The calculated band structure is unfolded into the Brillouin zone for $SrIrO_3$ without distortion [Fig. 1(a)] using the code BandUP.[21,22]

III. SURFACE TERMINATION

From the x-ray photoemission spectra, we find that the topmost Sr–O surface layer is distinct from the bulk. Confirmation that the surface termination of $SrIrO_3$(001) is Sr–O comes from plotting the Sr to Ir core level intensity as a function of emission angle. In Fig. 3, the Sr 3d to the Ir 4f core level photoemission intensities have been plotted, as a function of emission angle. This ratio increases at the very highest take-off angles, which in turn are the most surface sensitive.[23–25] For a conductive oxide like $SrIrO_3$, the electron mean free path varies from about 15 Å at 0° to about 2.6 Å at 80° incident angle for an electron kinetic energy of about 1300 eV,

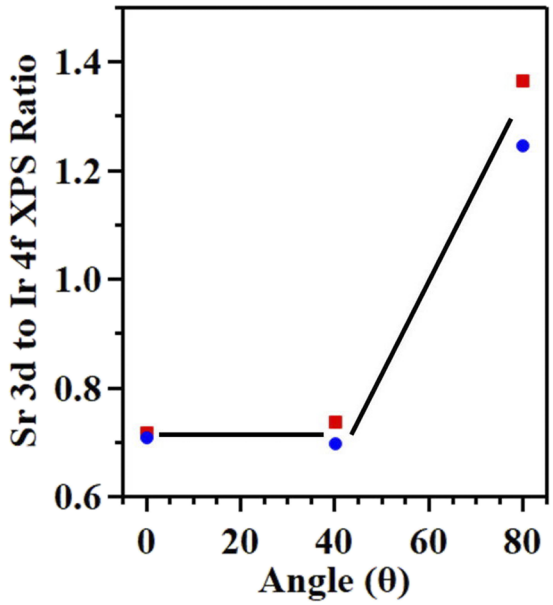

FIG. 3. The Sr 3d core level to the combined Ir 4f and $5p_{1/2}$ core level photoemission intensities plotted as a function of angle. The emission angles are all with respect to the surface normal. Several successive sample annealing treatments, at ~150 °C, change the surface stoichiometry only slightly: red are the intensity ratios taken before and blue are taken after annealing.

because as this system is metallic, there are plasmon electron kinetic energy loss mechanisms. Since the larger take-off angles are highly surface sensitive, this tends to suggest that the surface is Sr–O terminated and suggests that there is a large difference in enthalpy between the surface and the bulk.

Several successive sample annealing treatments, at ~150 °C, change the surface stoichiometry only slightly, as is evident in the Sr 3d to the Ir 4f core level photoemission intensities. This is despite that annealing the surface successively leads to elimination of the expected C_{4v} LEED pattern, possibly as a result of IrO_2 sublimation.[9,26] The very sharp increase in the relative Sr 3d intensity and increase in the core level binding energy suggest that the surface electronic structure, due to the Sr–O termination, is extremely thin and restricted to the topmost surface. This Sr–O surface termination, observed here, is consistent with prior growth studies where a "self-organized" conversion of the surface termination from IrO_2 to SrO occurs during the initial growth of $SrIrO_3$[9] and from RuO_2 to Sr–O in the growth of $SrRuO_3$.[26]

Recent transport studies have shown that the critical thickness for a metal–insulator transition is 4 unit cells in bare $SrIrO_3$ thin films[15] and 3 unit cells in $SrIrO_3$ films encapsulated by $SrTiO_3$ top layers,[11] which clearly illustrate the potential influence of the surface layer at the atomic scale. In this regard, $SrIrO_3$ differs significantly from other oxides, like strontium perovskites,[27] where the Sr enrichment at the surface persists well away from the surface. Additionally, unlike many other oxides or perovskites, the surface of $SrIrO_3$ is incredibly fragile. Changes in vacuum conditions and modest annealing were seen to lead to a reduction or loss of surface order, as observed in LEED.

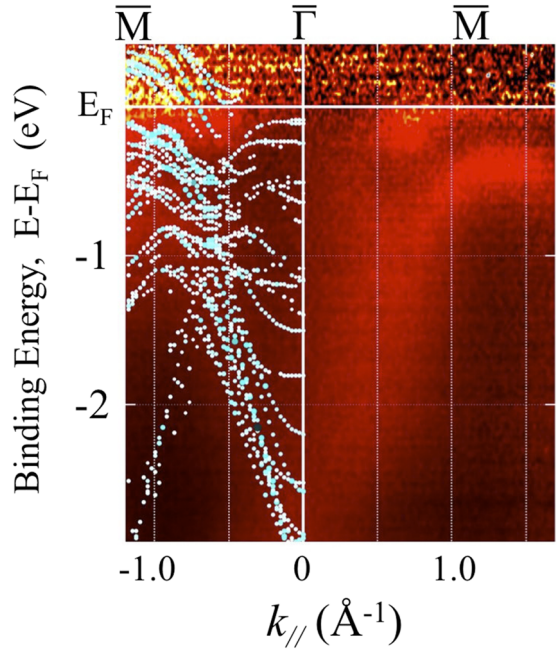

FIG. 4. The experimental valence band electronic structure of a 5 nm thick orthorhombic $SrIrO_3$(001) thin film as derived from angle-resolved photoemission, taken at room temperature with a photon energy of 150 eV. Superimposed on experiment are the results from the DFT calculated band structure, on the left (light blue circles mark a large contribution to the spectral weight).

Despite the strong surface to bulk core level shift of Sr, in the Sr–O surface layer, the experimental band structure probed via HR-ARPES is consistent with unreconstructed $SrIrO_3$(001). Figure 4 shows the band structure of $SrIrO_3$(001) from the $\bar{\Gamma}$ (surface Brillouin center) to the $\bar{M}$ point (the edge of the surface Brillouin zone). This experimental band structure (Fig. 4) is consistent with the semimetallic character of $SrIrO_3$, in excellent agreement with previous reports on orthorhombic $SrIrO_3$ thin films,[7–9,12] and very different from the distorted hexagonal $SrIrO_3$.[6] Superimposed on the experimental data along -*k* are the DFT calculations of bulk orthorhombic $SrIrO_3$, which well captures the position and energy levels of the heavy and light hole bands. There is clear evidence for an occupied density of states near the measured Fermi level (E_F), which is away from the Brillouin center at 0.7 $Å^{-1}$, as well as significant dispersion of the occupied bands, symmetric about the Brillouin zone edge.[7–9] The Brillouin zone critical $\bar{M}$ point placement is also consistent with a_o = 3.905 Å for $SrTiO_3$. We have increased the energy window of the calculated band structure by a factor of 1.2, to improve the match between theory (left) and experiment (right) in Fig. 4. The surface Brillouin zone from the band structure is consistent with the unfolded $SrIrO_3$(001), i.e., a tetragonal $SrIrO_3$(001), similar to previous reports.[9]

IV. SUPER-PERIODICITY

Figure 1(a) shows $SrIrO_3$ having the hypothetic perovskite crystal structure without distortion. The black box in Fig. 1(a) denotes the ideal cubic perovskite unit cell. Figure 1(b) exhibits the real crystal structure of a $SrIrO_3$ thin film with octahedral distortion.[12] This distortion leads to the orthorhombic unit cell ($\sqrt{2}a_o \times 2a_o \times \sqrt{2}a_o$), as shown in Fig. 1(b). The resulting Brillouin zone is also shown in Fig. 1(c) (the small purple volume). In a previous study, Schütz and colleagues[9] found in their LEED studies a 2 × 2 super-periodicity [p(2 × 2)] for 4 unit cell thick films, and a centered 2 × 2 super-periodicity [i.e., a c(2 × 2) in real space or $\left(\sqrt{2}/2\right) \times \left(\sqrt{2}/2\right)$ R45° in reciprocal space] for a 3 unit cell thick film. In contrast, the LEED image in Fig. 2(b) shows evidence for a super-periodicity that differs from both of these two aforementioned super-structures.[9] In fact, the extra diffraction spots in LEED for these orthorhombic $SrIrO_3$(001) films can be described as a $\left(\sqrt{2}/4\right) \times \left(\sqrt{2}/4\right)$ R45° reciprocal space structure, as indicated by the extra diffraction spots in the LEED. The super-position of orthogonal rectangular lattice domains, also with a super-periodicity, cannot be excluded either as the origin of the additional diffraction beams observed in the LEED [Fig. 2(b)]. Precise determination of the origin of the super-periodicity would be aided by intensity vs voltage analysis of the LEED or additional diffraction studies. Considering the cubic symmetry of the $SrTiO_3$ substrate, such a super-periodicity can originate either from a surface reconstruction or from lattice twining of a rectangular distortion due to the collective rotation and tilt of the Ir–O_6 octahedral,[9] at the subsurface layer.

To clarify which scenario can apply to our system, we combined the LEED data with the HR-ARPES results. Due to the large scattering cross section of Ir, the penetration depth of LEED (31.5 eV electron energy) could be deeper than the photoemission mean free path at 150 eV: although very material dependent, the electron mean free path frequently increases rapidly at kinetic energies below 50 eV, but rises only slowly at kinetic energies higher than 50 eV.[25] This is distinct from the LEED study shown in Ref. 9, which is performed at a much higher electron energy (120 eV) and thus more surface sensitive. Therefore, the fact that there is little evidence of band folding in the band structure, shown in Fig. 4, suggests that the topmost surface layer is not subject to a surface reconstruction at room temperature, and that the super-periodicity arises well away from the surface region. The explanation is that the angle-resolved photoemission is not influenced by multiple diffraction effects of the Sr–O top layer. Schütz *et al.*[9] attributed the $\left(\sqrt{2}/2\right) \times \left(\sqrt{2}/2\right)$ R45° reciprocal space structure for insulating $SrIrO_3$ to a substrate clamping effect, which suppresses the Ir–O_6 octahedral distortions. Assuming a similar clamping effect exists in our 5 nm (12.5 unit cells) films, the observed $\left(\sqrt{2}/4\right) \times \left(\sqrt{2}/4\right)$ R45° reciprocal space structure reveals a transition region from the interfacial layer (3 unit cells) to the topmost surface layer. The evolving crystal symmetry with distance from the substrate in this thickness range has previously been observed in epitaxial manganite thin films,[28] which has been attributed to competing misfit relaxation mechanisms. As orthorhombic $SrIrO_3$ is metastable in the bulk, such dislocations/misfit can form due to the evolving lattice symmetry.[10,29] Another possible scenario is the heterogeneous placement of IrO_6 oxygen octahedra tilts across the 12 monolayers film, which can possess certain super-periodicity, although a super-periodicity near the surface appears excluded by the placement of the Brillouin zone edge in the band mapping. The lattice distortion can have pronounced

impact on the electronic and magnetic properties of ultrathin $SrIrO_3$ films, and further affect the performance of $SrIrO_3$-based electronic devices.[29,30]

V. CONCLUSIONS

In conclusion, we have investigated the surface termination, electronic structure, and crystal symmetry of strained orthorhombic $SrIrO_3$(001) thin films on $SrTiO_3$ substrates. The Sr–O terminated surface states could contribute to the thickness-driven metal–insulator transition. While there is evidence in low energy electron diffraction of a super-periodicity, no band folding is seen in the experimental band structure, indicating the absence of surface reconstruction. The observed super-periodicity is attributed to a distortion of the orthorhombic structure well into the film, which may originate from the misfit relaxation from the epitaxial strain.

ACKNOWLEDGMENTS

This work was supported by NSF through the Nebraska Materials Research Science and Engineering Center (MRSEC), Grant No. DMR-1420645 (structural, spectroscopy, and DFT studies), NSF, Grant No. DMR-1710461 (sample growth and characterization), and the Semiconductor Research Corporation (SRC) under GRC Task No. 2831.001 (modeling). The research was performed in part in the Nebraska Nanoscale Facility: National Nanotechnology Coordinated Infrastructure and the Nebraska Center for Materials and Nanoscience, which are supported by the National Science Foundation under Award No. ECCS: 1542182, and the Nebraska Research Initiative. The experiments have been performed under the approval of HiSOR (Proposal No. 18BG005 and 18BG006).

DATA AVAILABILITY

The data that support the findings of this study are available from the corresponding author upon reasonable request.

REFERENCES

[1] Q. Wang, Y. Cao, J. A. Waugh, S. R. Park, T. F. Qi, O. B. Korneta, G. Cao, and D. S. Dessau, Phys. Rev. B **87**, 245109 (2013).
[2] D. Pincini, J. G. Vale, C. Donnerer, A. de la Torre, E. C. Hunter, R. Perry, M. Moretti Sala, F. Baumberger, and D. F. McMorrow, Phys. Rev. B **96**, 075162 (2017).
[3] G. Chen and M. Hermele, Phys. Rev. B **86**, 235129 (2012).
[4] B. J. Kim, H. Jin, S. J. Moon, J. Y. Kim, B. G. Park, C. S. Leem, J. Yu, T. W. Noh, C. Kim, S. J. Oh, J. H. Park, V. Durairaj, G. Cao, and E. Rotenberg, Phys. Rev. Lett. **101**, 076402 (2008).
[5] S. J. Moon, H. Jin, K. W. Kim, W. S. Choi, Y. S. Lee, J. Yu, G. Cao, A. Sumi, H. Funakubo, C. Bernhard, and T. W. Noh, Phys. Rev. Lett. **101**, 226402 (2008).
[6] T. Takayama, A. N. Yaresko, and H. Takagi, J. Phys.: Condens. Matter **31**, 074001 (2019).
[7] Z. T. Liu, M. Y. Li, Q. F. Li, J. S. Liu, W. Li, H. F. Yang, Q. Yao, C. C. Fan, X. G. Wan, Z. Wang, and D. W. Shen, Sci. Rep. **6**, 30309 (2016).
[8] Y. F. Nie, P. D. C. King, C. H. Kim, M. Uchida, H. I. Wei, B. D. Faeth, J. P. Ruf, J. P. C. Ruff, L. Xie, X. Pan, C. J. Fennie, D. G. Schlom, and K. M. Shen, Phys. Rev. Lett. **114**, 016401 (2015).
[9] P. Schütz, D. Di Sante, L. Dudy, J. Gabel, M. Stübinger, M. Kamp, Y. Huang, M. Capone, M. A. Husanu, V. N. Strocov, G. Sangiovanni, M. Sing, and R. Claessen, Phys. Rev. Lett. **119**, 256404 (2017).
[10] L. Zhang, B. Pang, Y. B. Chen, and Y. Chen, Crit. Rev. Solid State Mater. Sci. **43**, 367 (2018).
[11] D. J. Groenendijk, C. Autieri, J. Girovsky, M. Carmen Martinez-Velarte, N. Manca, G. Mattoni, A. M. R. V. L. Monteiro, N. Gauquelin, J. Verbeeck, A. F. Otte, M. Gabay, S. Picozzi, and A. D. Caviglia, Phys. Rev. Lett. **119**, 256403 (2017).
[12] J. Liu, D. Kriegner, L. Horak, D. Puggioni, C. Rayan Serrao, R. Chen, D. Yi, C. Frontera, V. Holy, A. Vishwanath, J. M. Rondinelli, X. Marti, and R. Ramesh, Phys. Rev. B **93**, 085118 (2016).
[13] J. M. Longo, J. A. Kafalas, and R. J. Arnott, J. Solid State Chem. **3**, 174 (1971).
[14] L. Zhang, Q. Liang, Y. Xiong, B. Zhang, L. Gao, H. Li, Y. B. Chen, J. Zhou, S.-T. Zhang, Z.-B. Gu, S.-h. Yao, Z. Wang, Y. Lin, and Y.-F. Chen, Phys. Rev. B **91**, 035110 (2015).
[15] L. Zhang, X. Jiang, X. Xu, and X. Hong, e-print arXiv:1907.11814 (2019).
[16] K. Shimada, M. Arita, Y. Takeda, H. Fujino, K. Kobayashi, T. Narimura, H. Namatame, and M. Taniguchi, Surf. Rev. Lett. **09**, 529 (2002).
[17] H. Iwasawa, K. Shimada, E. F. Schwier, M. Zheng, Y. Kojima, H. Hayashi, J. Jiang, M. Higashiguchi, Y. Aiura, H. Namatame, and M. Taniguchi, Synchrotron Radiat. **24**, 836 (2017).
[18] D. Vanderbilt, Phys. Rev. B **41**, 7892 (1990).
[19] P. Giannozzi *et al.*, J. Phys.: Condens. Matter **21**, 395502 (2009).
[20] J. P. Perdew, K. Burke, and M. Ernzerhof, Phys. Rev. Lett. **77**, 3865 (1996).
[21] P. V. C. Medeiros, S. Stafström, and J. Björk, Phys. Rev. B **89**, 041407(R) (2014).
[22] P. V. C. Medeiros, S. S. Tsirkin, S. Stafström, and J. Björk, Phys. Rev. B **91**, 041116(R) (2015).
[23] D. Briggs and M. P. Seah, *Practical Surface Analysis, Auger and X-Ray Photoelectron Spectroscopy* (Wiley, Chichester, 1996).
[24] W. F. Egelhoff, Surf. Sci. Rep. **6**, 253 (1987).
[25] M. P. Seah and W. A. Dench, Surf. Interface Anal. **1**, 2 (1979).
[26] G. Rijnders, D. H. A. Blank, J. Choi, and C.-B. Eom, Appl. Phys. Lett. **84**, 505 (2004).
[27] H. Dulli, P. A. Dowben, S.-H. Liou, and E. W. Plummer, Phys. Rev. B **62**, R14629 (2000).
[28] F. Sandiumenge, J. Santiso, L. Balcells, Z. Konstantinovic, J. Roqueta, A. Pomar, J. P. Espinos, and B. Martınez, Phys. Rev. Lett. **110**, 107206 (2013).
[29] L. Zhang, H. J. Gardner, X. G. Chen, V. R. Singh, and X. Hong, J. Phys.: Condens. Matter **27**, 132201 (2015).
[30] L. Zhang, X. G. Chen, H. J. Gardner, M. A. Koten, J. E. Shield, and X. Hong, Appl. Phys. Lett. **107**, 152906 (2015).